Proceedings of the
44th IEEE Conference on Decision and Control, and
the European Control Conference 2005
Seville, Spain, December 12-15, 2005

Duhem Models for Hysteresis in Sliding and Presliding Friction*

JinHyoung Oh[†], Ashwani K. Padthe[†], Dennis S. Bernstein[†], Demosthenis D. Rizos[‡], and Spilios D. Fassois[‡]

[†]Department of Aerospace Engineering, The University of Michigan,
Ann Arbor, MI 48109-2140, USA, {johzz,dsbaero}@umich.edu

[‡]Department of Mechanical Engineering and Aeronautics, The University of Patras,
GR 265 00, Patras, Greece, {driz,fassois}@mech.upatras.gr

Abstract— **In this paper we analyze the Dahl, LuGre, and Maxwell-slip friction models as Duhem hysteresis models. We classify each model as either a generalized or a semilinear Duhem model, and we analyze the rate-independent or rate-dependent behavior of the corresponding input-output map. This unified treatment of Duhem-based friction models is used to investigate friction-induced hysteresis.**

I. Introduction

Friction is a dynamic phenomenon of widespread importance, and the associated literature is vast; overviews are given in [1]–[3]. Friction can be viewed as an emergent, macroscopic phenomenon arising from molecular interaction. Consequently, both phenomenological (physics-based) and empirical (experiment-based) models have been proposed [2], [4]–[10]. Estimation and control methods have been developed for applications involving friction [11]–[14]; however, these topics are beyond the scope of this paper.

In friction modeling it is important to distinguish between *presliding friction* and *sliding friction*. Presliding or *micro-slip* friction refers to the friction forces that occur when the relative displacement between two contacting surfaces is microscopic. Sliding friction refers to the friction forces that occur when the relative displacement is macroscopic.

From a mathematical point of view, friction modeling is challenging since some models involve nonsmooth dynamics. For example, the most widely used dry friction model, namely, Coulomb friction, is discontinuous. Discontinuous dry friction models are studied in [15]. Some friction models are continuous but not Lipschitzian, in which case finite settling time is possible.

Understanding presliding friction is important for high precision position control applications. For example, hysteresis can occur between the presliding friction force and displacement [5], [8], [9]. As a dynamic phenomenon, hysteresis is the result of *multistability*, which refers to the existence of multiple attracting equilibria [16]–[18]. Hysteresis is a quasi-static phenomenon in the sense that the hysteresis map is the limit of the dynamic input-output maps as the period of the periodic input becomes unbounded. In both presliding and sliding friction models, there exist multiple equilibria corresponding to states that model the friction forces under constant displacement or velocity.

*This research was supported in part by the National Science Foundation under grant ECS–0225799.

The goal of the present paper is to examine some well-known friction models from a hysteresis modeling point of view. Our starting point is [19], which focuses on the Duhem model for hysteresis. The Duhem model has the property that, under constant inputs, every state is an equilibrium. When there exist multiple attracting (step-convergent) equilibria for a step input, the system exhibits hysteresis under inputs that drive the system through distinct equilibria that map into distinct outputs. In certain cases, the limiting input-output map is independent of the input period; this case is known as *rate-independent* hysteresis. In general, the hysteresis map is *rate-dependent*, although the terminology is slightly misleading since, as already noted, hysteresis per se is a quasi-static phenomenon.

The generalized Duhem model $\dot{x} = f(x,u)g(\dot{u})$ and a specialization known as the *semilinear Duhem model*, whose dynamics are of the form $\dot{x} = (Ax+Bu)g(\dot{u})$, are considered in [19]. These models give rise to rate-independent hysteresis when the function g is positively homogeneous; otherwise, the hysteresis is usually rate-dependent.

In the present paper we consider three friction models, namely, the Dahl model, the LuGre model, and the Maxwell-slip model. We recast each model in the form of a generalized or a semilinear Duhem model and provide a unified framework for comparing the hysteretic nature of these models. For example, the Dahl model is shown to be a rate-independent generalized Duhem model. Furthermore, in one special case, the Dahl model is also a semilinear Duhem model for which closed-form solutions are available. Similarly, the LuGre model can be seen to be a rate-dependent generalized Duhem model.

The contents of the paper are as follows. In Section 2 we review the basic theory of the Duhem model. In sections 3, 4, and 5 we recast the Dahl, LuGre, and Maxwell-slip models as Duhem models and relate their dynamic behavior to properties of the Duhem models. In Section 6 we study the sliding friction dynamics of the three friction models. In section 7 we provide some concluding remarks.

II. Generalized and Semilinear Duhem Models

In this section, we summarize the main result of [19] concerning the generalized and semilinear Duhem models. The terms closed curve, limiting periodic input-output map, hysteresis map, and rate-independence are defined in [19].

0-7803-9568-9/05/$20.00 ©2005 IEEE

Consider the single-input single-output *generalized Duhem model* given by

$$\dot{x}(t) = f\big(x(t), u(t)\big)g\big(\dot{u}(t)\big), \qquad x(0) = x_0, \quad t \geq 0, \tag{1}$$

$$y(t) = h\big(x(t), u(t)\big), \tag{2}$$

where $x : [0, \infty) \to \mathbb{R}^n$ is absolutely continuous, $u : [0, \infty) \to \mathbb{R}$ is continuous and piecewise C^1, $f : \mathbb{R}^n \times \mathbb{R} \to \mathbb{R}^{n \times r}$ is continuous, $g : \mathbb{R} \to \mathbb{R}^r$ is continuous and satisfies $g(0) = 0$, $y : [0, \infty) \to \mathbb{R}$, and $h : \mathbb{R}^n \times \mathbb{R} \to \mathbb{R}$ is continuous. The value of $\dot{x}(t)$ at a point t at which $\dot{u}(t)$ is discontinuous can be assigned arbitrarily. We assume that the solution to (1) exists and is unique on all finite intervals. Under these assumptions, x and y are continuous and piecewise C^1. The following result in [19] is needed for further discussion.

Proposition 2.1:. Assume that g is positively homogeneous, that is, $g(\alpha v) = \alpha g(v)$ for all $\alpha > 0$ and $v \in \mathbb{R}$. Then the generalized Duhem model (1), (2) is rate independent.

As shown in [19], if g is positively homogeneous, then there exist $h_+, h_- \in \mathbb{R}^r$ such that

$$g(v) = \begin{cases} h_+ v, & v \geq 0, \\ h_- v, & v < 0, \end{cases} \tag{3}$$

and the rate-independent generalized Duhem model (1), (2) can be reparameterized in terms of u. Specifically, consider

$$\frac{\mathrm{d}\hat{x}(u)}{\mathrm{d}u} = \begin{cases} f_+(\hat{x}(u), u), & \text{when } u \text{ increases}, \\ f_-(\hat{x}(u), u), & \text{when } u \text{ decreases}, \\ 0, & \text{otherwise}, \end{cases} \tag{4}$$

$$\hat{y}(u) = h\big(\hat{x}(u), u\big), \tag{5}$$

for $u \in [u_{\min}, u_{\max}]$ and with initial condition $\hat{x}(u_0) = x_0$, where $f_+(x, u) \triangleq f(x, u)h_+$, $f_-(x, u) \triangleq f(x, u)h_-$, and $u_0 \in [u_{\min}, u_{\max}]$. Then $x(t) \triangleq \hat{x}(u(t))$ and $y(t) \triangleq \hat{y}(u(t))$ satisfy (1), (2). Note that the reparameterized Duhem model (4) and (5) can be viewed as a time-varying dynamical system with nonmonotonic time u.

As a specialization of (1) and (2), we now consider the *rate-independent semilinear Duhem model*

$$\dot{x}(t) = \begin{bmatrix} \dot{u}_+(t) I_n & \dot{u}_-(t) I_n \end{bmatrix} \times \left(\begin{bmatrix} A_+ \\ A_- \end{bmatrix} x(t) + \begin{bmatrix} B_+ \\ B_- \end{bmatrix} u(t) + \begin{bmatrix} E_+ \\ E_- \end{bmatrix} \right), \tag{6}$$

$$y(t) = Cx(t) + Du(t), \qquad x(0) = x_0, \quad t \geq 0, \tag{7}$$

where $A_+ \in \mathbb{R}^{n \times n}$, $A_- \in \mathbb{R}^{n \times n}$, $B_+ \in \mathbb{R}^n$, $B_- \in \mathbb{R}^n$, $E_+ \in \mathbb{R}^n$, $E_- \in \mathbb{R}^n$, $C \in \mathbb{R}^{1 \times n}$, $D \in \mathbb{R}$, and

$$\dot{u}_+(t) \triangleq \max\{0, \dot{u}(t)\}, \quad \dot{u}_-(t) \triangleq \min\{0, \dot{u}(t)\}. \tag{8}$$

Let $\rho(A)$ denote the spectral radius of $A \in \mathbb{R}^{n \times n}$, and let the *limiting input-output map* $\mathcal{F}_\infty(u, y)$ be the set of points $z \in \mathbb{R}^2$ such that there exists an increasing, divergent sequence $\{t_i\}_{i=1}^\infty$ in $[0, \infty)$ satisfying $\lim_{i \to \infty} \|(u(t_i), y(t_i)) - z\| = 0$. The following result given in [19] provides a sufficient condition for the existence of the limiting periodic input-output map of a rate-independent semilinear Duhem model.

Theorem 2.1:. Consider the rate-independent semilinear Duhem model (6), (7), where $u : [0, \infty) \to [u_{\min}, u_{\max}]$ is continuous, piecewise C^1, and periodic with period α and has exactly one local maximum $u_{\max}$ in $[0, \alpha)$ and exactly one local minimum $u_{\min}$ in $[0, \alpha)$. Furthermore, define $\beta \triangleq u_{\max} - u_{\min}$, and assume that A_+ and A_- are invertible, and

$$\rho\left(e^{\beta A_+} e^{-\beta A_-}\right) < 1. \tag{9}$$

Then, (6) has a unique periodic solution $x : [0, \infty) \to \mathbb{R}^n$, the limiting periodic input-output map $\mathcal{H}_\infty(u)$ exists, and the limiting input-output map $\mathcal{F}_\infty(u, y)$ is given by $\mathcal{F}_\infty(u, y) = \mathcal{H}_\infty(u)$. Specifically,

$$\begin{aligned} \mathcal{H}_\infty(u) = {} & \left\{ \big(u, \hat{y}_+(u)\big) \in \mathbb{R}^2 : u \in [u_{min}, u_{max}] \right\} \\ & \cup \left\{ \big(u, \hat{y}_-(u)\big) \in \mathbb{R}^2 : u \in [u_{min}, u_{max}] \right\}, \end{aligned} \tag{10}$$

where

$$\hat{y}_+(u) = Ce^{A_+(u - u_{\min})}\hat{x}_+ - C\mathcal{Z}_+(u, u_{\min}) + Du,$$

$$\hat{y}_-(u) = Ce^{A_-(u - u_{\max})}\hat{x}_- - C\mathcal{Z}_-(u, u_{\max}) + Du,$$

and

$$\begin{aligned} \hat{x}_+ \triangleq {} & -\left(I - e^{-\beta A_-} e^{\beta A_+}\right)^{-1} \times \\ & \left(e^{-\beta A_-}\mathcal{Z}_+(u_{\max}, u_{\min}) + \mathcal{Z}_-(u_{\min}, u_{\max})\right), \\ \hat{x}_- \triangleq {} & -\left(I - e^{\beta A_+} e^{-\beta A_-}\right)^{-1} \times \\ & \left(e^{\beta A_+}\mathcal{Z}_-(u_{\min}, u_{\max}) + \mathcal{Z}_+(u_{\max}, u_{\min})\right), \\ \mathcal{Z}_+(u, u_0) \triangleq {} & A_+^{-1}(uI - u_0 e^{A_+(u-u_0)})B_+ + A_+^{-2} \times \\ & (I - e^{A_+(u-u_0)})B_+ + A_+^{-1}(I - e^{A_+(u-u_0)})E_+, \\ \mathcal{Z}_-(u, u_0) \triangleq {} & A_-^{-1}(uI - u_0 e^{A_-(u-u_0)})B_- + A_-^{-2} \times \\ & (I - e^{A_-(u-u_0)})B_- + A_-^{-1}(I - e^{A_-(u-u_0)})E_-. \end{aligned}$$

III. Dahl Model

The Dahl model [4] is a nonlinear friction model of the form

$$\dot{F}(t) = \sigma \left| 1 - \frac{F(t)}{F_{\mathrm{C}}} \operatorname{sgn} \dot{u}(t) \right|^\gamma \operatorname{sgn}\left(1 - \frac{F(t)}{F_{\mathrm{C}}} \operatorname{sgn} \dot{u}(t)\right) \dot{u}(t), \tag{11}$$

where F is the friction force, u is the relative displacement between the two surfaces in contact, $F_{\mathrm{C}} > 0$ is the Coulomb friction force, $\gamma \geq 0$ is a parameter that determines the force-deflection curve, and $\sigma > 0$ is the rest stiffness, that is, the slope of the force-deflection curve when $F = 0$. The right hand side of (11) is Lipschitz continuous in F for $\gamma \geq 1$ but not Lipschitz in F for $0 \leq \gamma < 1$.

When u is increasing, the right-hand side of (11) is positive for all $F < F_{\mathrm{C}}$ and negative for all $F > F_{\mathrm{C}}$. Similarly when u is decreasing, the right-hand side of (11) is positive for all $F < -F_{\mathrm{C}}$ and negative for all $F > -F_{\mathrm{C}}$. Hence the friction force F asymptotically approaches the Coulomb friction force under monotonic inputs. The parameter γ determines the shape of the input-output map. The input-output hysteresis maps of the Dahl model for

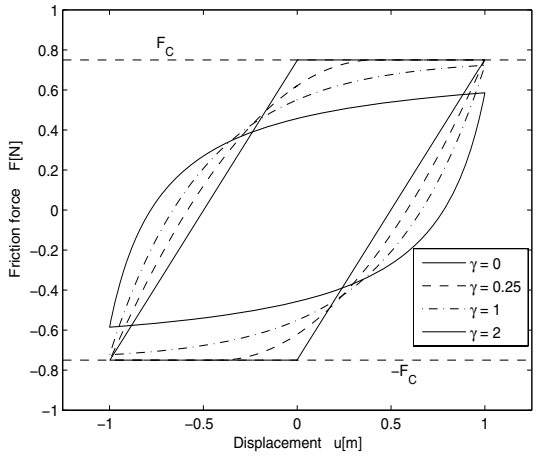

Fig. 1. Displacement u versus the friction force F for the Dahl model with various values of γ, where $F_{\rm C} = 0.75$ N, $\sigma = 7.5$ N/m, and $u(t) = 10^{-5} \sin 0.1t$ m.

various values of γ are shown in Figure 1. In practice, γ is typically set to 0 or 1 [7], [20].

To represent (11) as a Duhem model, let

$$\mathcal{F}_+\big(F(t)\big) \triangleq \sigma \left|1 - \frac{F(t)}{F_c}\right|^{\gamma} \operatorname{sgn}\left(1 - \frac{F(t)}{F_c}\right), \tag{12}$$

$$\mathcal{F}_-\big(F(t)\big) \triangleq \sigma \left|1 + \frac{F(t)}{F_c}\right|^{\gamma} \operatorname{sgn}\left(1 + \frac{F(t)}{F_c}\right). \tag{13}$$

Then the Dahl model (11) can be rewritten as

$$\dot{F}(t) = \sigma \begin{bmatrix} \mathcal{F}_+\big(F(t)\big) & \mathcal{F}_-\big(F(t)\big) \end{bmatrix} \begin{bmatrix} \dot{u}_+(t) \\ \dot{u}_-(t) \end{bmatrix}, \tag{14}$$

which is a generalized Duhem model for all $\gamma \geq 0$. Furthermore, since $\begin{bmatrix} \dot{u}_+(t) & \dot{u}_-(t) \end{bmatrix}^{\rm T}$ is positively homogeneous, Proposition 2.1 implies that (14) is rate independent for all $\gamma \geq 0$.

Let $\gamma = 1$. Then (11) becomes

$$\begin{aligned} \dot{F}(t) &= \sigma \left(1 - \frac{F(t)}{F_C} \operatorname{sgn} \dot{u}(t)\right) \dot{u}(t) \\ &= \begin{bmatrix} -\frac{\sigma}{F_C} F(t) + \sigma & \frac{\sigma}{F_C} F(t) + \sigma \end{bmatrix} \begin{bmatrix} \dot{u}_+(t) \\ \dot{u}_-(t) \end{bmatrix}, \end{aligned}$$

which is a rate-independent semilinear Duhem model. Furthermore, the convergence condition (9) becomes

$$e^{-2\frac{\beta\sigma}{F_{\rm C}}} < 1. \tag{15}$$

Taking logarithm on both sides of (15), we have,

$$-2\frac{\beta\sigma}{F_{\rm C}} < 0, \tag{16}$$

which is true if and only if $\beta > 0$. We thus have the following result as a direct consequence of Theorem 2.1.

Corollary 3.1:. Consider the Dahl model (11) with $\gamma = 1$. Let u be continuous, piecewise $\rm C^1$, and periodic with period α and have exactly one local maximum $u_{\max}$ in $[0, \alpha)$ and exactly one local minimum $u_{\min}$ in $[0, \alpha)$. Then (16) is true, (11) has a unique periodic solution $F : [0, \infty) \to \mathbb{R}^n$, the limiting periodic input-output map $\mathcal{H}_\infty(u)$ exists, and the limiting input-output map $\mathcal{F}_\infty(u, F)$ is given by $\mathcal{F}_\infty(u, F) = \mathcal{H}_\infty(u)$. Specifically,

$$\begin{aligned} \mathcal{H}_\infty(u) = &\left\{ \big(u, \hat{F}_+(u)\big) \in \mathbb{R}^2 : u \in [u_{min}, u_{max}] \right\} \\ &\cup \left\{ \big(u, \hat{F}_-(u)\big) \in \mathbb{R}^2 : u \in [u_{min}, u_{max}] \right\}, \end{aligned} \tag{17}$$

where

$$\hat{F}_+(u) = e^{-\frac{\sigma}{F_{\rm C}}(u - u_{\min})} \hat{\alpha}_+ + F_{\rm C} \left(1 - e^{-\frac{\sigma}{F_{\rm C}}(u - u_{\min})}\right),$$

$$\hat{F}_-(u) = e^{\frac{\sigma}{F_{\rm C}}(u - u_{\max})} \hat{\alpha}_- - F_{\rm C} \left(1 - e^{-\frac{\sigma}{F_{\rm C}}(u - u_{\max})}\right),$$

and

$$\hat{\alpha}_+ = -\hat{\alpha}_- = F_{\rm C} \frac{e^{\frac{-\beta\sigma}{F_{\rm C}}} - 1}{e^{-\frac{\beta\sigma}{F_{\rm C}}} + 1}.$$

IV. LuGre Model

The *LuGre model* [7], which models the asperities of two surfaces as elastic bristles, is given by

$$\dot{x}(t) = \dot{u}(t) - \frac{|\dot{u}(t)|}{r\big(\dot{u}(t)\big)} x(t), \tag{18}$$

$$F(t) = \sigma_0 x(t) + \sigma_1 \dot{x}(t) + \sigma_2 \dot{u}(t), \tag{19}$$

where x is the average deflection of the bristles, u is the relative displacement, F is the friction force, and $\sigma_0, \sigma_1, \sigma_2 > 0$ are stiffness, damping, and viscous friction coefficients, respectively. The right hand side of 18 is Lipschitz continuous in x.

There are various choices for the function $r(\dot{u}(t))$ given in [1, p. 83]. In [7] $r(\dot{u}(t))$ is defined by

$$r(\dot{u}(t)) = \frac{F_{\rm C}}{\sigma_0} + \frac{F_{\rm S} - F_{\rm C}}{\sigma_0} e^{-(\dot{u}(t)/v_{\rm S})^2}, \tag{20}$$

where $F_{\rm C} > 0$ is the Coulomb friction force, $F_{\rm S}$ is the stiction (sticking friction) force, and $v_{\rm S}$ is the Stribeck velocity, which is the velocity at which the plot of the steady state friction force versus velocity starts dipping. For a given constant velocity, the steady state friction force F_{ss}, derived from the Lugre model, is given by

$$F_{ss}(\dot{u}(t)) = \sigma_0 r(\dot{u}(t)) \operatorname{sgn}(\dot{u}(t)) + \sigma_2 \dot{u}(t). \tag{21}$$

A plot of steady state friction force against velocity is shown in Figure 2. The dip in the friction force at low magnitudes of velocity is the Stribeck effect.

If $r(\dot{u}(t)) = F_{\rm C}$, $\sigma_0 = 1$, and $\sigma_1 = \sigma_2 = 0$, then (18), (19) are equivalent to the Dahl model (11) with $\gamma = 1$ and $\sigma = 1$. The Dahl model is basically Coulomb friction with a lag in the change of the friction force when the direction of motion reverses. The Lugre model combines the friction lag of the Dahl model with the Stribeck effect.

The state equations (18) and (19) can be rewritten as

$$\dot{x}(t) = \begin{bmatrix} 1 & x(t) \end{bmatrix} \begin{bmatrix} \dot{u}(t) \\ -\frac{|\dot{u}(t)|}{r\big(\dot{u}(t)\big)} \end{bmatrix}, \tag{22}$$

$$y(t) = \sigma_0 x(t) + \sigma_1 \dot{x}(t) + \sigma_2 \dot{u}(t), \tag{23}$$

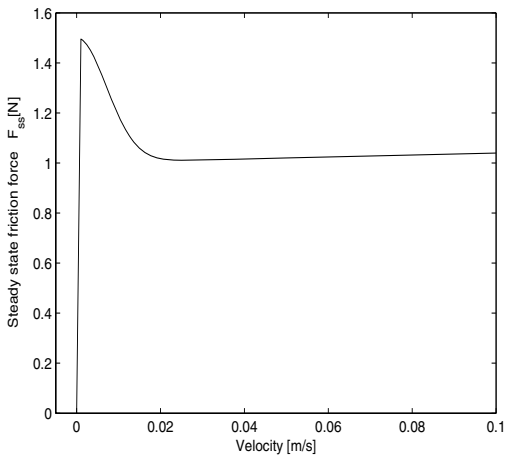

Fig. 2. Steady state friction force (21) given by the Lugre model, where $F_{\rm C} = 1$ N, $F_{\rm S} = 1.5$ N, $v_{\rm S} = 0.001$ m/s, $\sigma_0 = 10^5$ N/m, and $\sigma_2 = 0.4$ N-s/m.

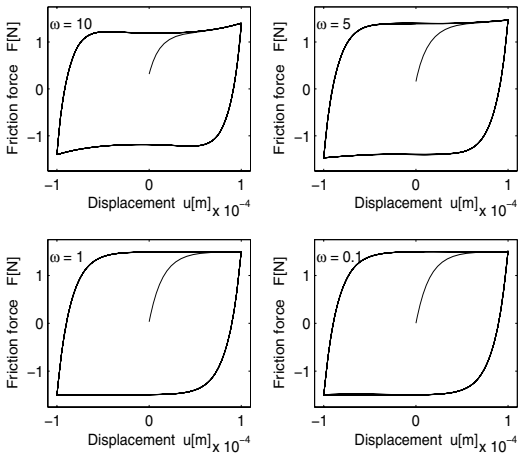

Fig. 3. Input-output maps for the LuGre model with $F_{\rm C} = 1$ N, $F_{\rm S} = 1.5$ N, $v_{\rm S} = 0.001$ m/s, $\sigma_0 = 10^5$ N/m, $\sigma_1 = \sqrt{10^5}$ N-s/m, $\sigma_2 = 0.4$ N-s/m, and $u(t) = 10^{-4} \sin \omega t$ m.

which is a generalized Duhem model of the form (1). Since r given in (20) is not positively homogeneous, the LuGre model is not necessarily rate independent. In fact, the input-output maps in Figure 3 show that the LuGre model is rate dependent.

V. Maxwell-Slip Model

The *Maxwell-slip model* [5], [9], [10] as shown in Figure 4, has N masses m_i with displacement x_i connected by a stiffness k_i to a common termination point whose displacement is u. Associated with each mass is a displacement deadband of width $\Delta_i \in \mathbb{R}$, below which the mass does not move, and above which the mass moves with velocity $\dot{u}$, that is, the inertia of the masses is ignored when the mass

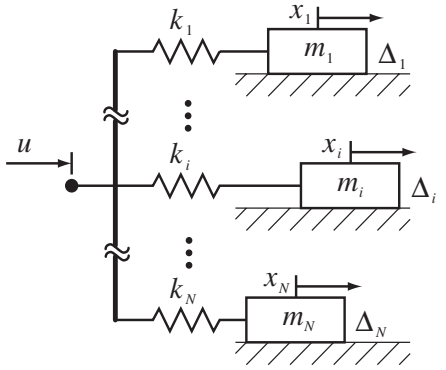

Fig. 4. The Maxwell slip model with N masses and N springs. Each mass is associated with a displacement deadband Δ_i, below which the mass does not move, and above which the mass moves with the same velocity as the common termination point.

is sliding. We can write this system as the Duhem model

$$\dot{x}_i(t) = \begin{bmatrix} \mathcal{M}\big(x_i(t),u(t),\Delta\big) & 1\text{–}\mathcal{N}\big(x_i(t),u(t),\Delta\big) \end{bmatrix} \begin{bmatrix} \dot{u}_+(t) \\ \dot{u}_-(t) \end{bmatrix} \tag{24}$$

$$F(t) = \textstyle\sum_{i=1}^{N} k_i\big(-x_i(t) + u(t)\big), \tag{25}$$

for $i = 1, \ldots, N$, where F is the friction force, $\Delta \triangleq [\Delta_1 \cdots \Delta_N]$,

$$\mathcal{M}\big(x_i,u,\Delta\big) \triangleq U\big(-x_i + u - \Delta_i\big), \tag{26}$$

$$\mathcal{N}\big(x_i,u,\Delta\big) \triangleq U\big(-x_i + u + \Delta_i\big), \tag{27}$$

and,
$$U(v) \triangleq \begin{cases} 1, & v \geq 0, \\ 0, & v < 0. \end{cases} \tag{28}$$

Illustrative input-output maps of the Maxwell-slip model for $N = 1$ and $N = 10$ are shown in Figures 5(a) and 5(b), respectively.

The Maxwell-slip model (24), (25) is a generalized Duhem model of the form (1), (2). Note that $\begin{bmatrix} \dot{u}_+(t) & \dot{u}_-(t) \end{bmatrix}^{\rm T}$ is positively homogeneous, and thus Proposition 2.1 implies that (24), (25) is rate independent. Since the function U and hence the functions $\mathcal{M}$ and $\mathcal{N}$ are discontinuous, the Maxwell-slip model is also discontinuous.

VI. Sliding Behavior of the Dahl, LuGre and Maxwell-slip Models

We now consider the behavior of the presliding friction models in the sliding regime, that is, the behavior of these models when subject to large magnitudes of displacement and velocity.

Consider the Dahl model (11) with $\gamma = 1$. The friction force F as a function of displacement u and velocity $\dot{u}$ is shown in Figure 6, where u and $\dot{u}$ have initial values equal to zero. The displacement is -20 when the velocity changes sign from negative to positive and is zero when the velocity changes sign from positive to negative. As noted in Section 4, Figure 6(b) shows that each velocity reversal leads to a change in the sign of the friction force but with a delay.

The friction force F as a function of displacement u and velocity $\dot{u}$ for the LuGre and Maxwell-slip models are shown

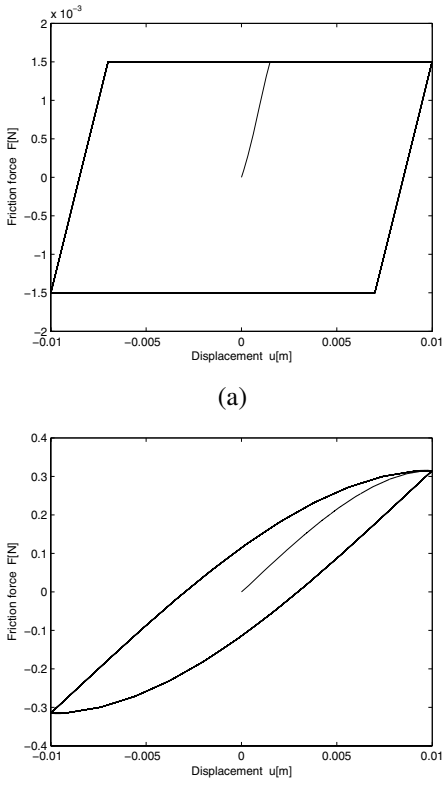

Fig. 5. Input-output map of the Maxwell-slip model (a) with $N = 1$, $\Delta_1 = 1.5 \times 10^{-3}$ m, $k_1 = 1$ N/m, $u(t) = 0.01 \sin 0.1t$ m, and (b) with $N = 10$, $\Delta = [1.5, 2.4, 3.3, 4.2, 5.1, 6, 6.9, 7.8, 8.7, 9.6] \times 10^{-3}$ m, $k = [1, 1.8, 2.6, 3.4, 4.2, 5, 5.8, 6.6, 7.4, 8.2]$ N/m, $u(t) = 0.01 \sin 0.1t$ m.

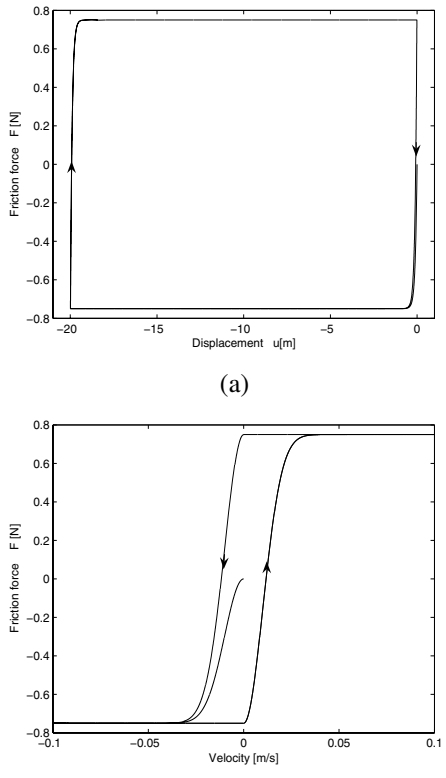

Fig. 6. (a) Friction force versus displacement and the corresponding (b) friction force versus velocity for the Dahl model with $F_{\rm C} = 0.75$ N, $\gamma = 1$, $\sigma = 7.5$ N/m, and $u(t) = 10\ (\cos 0.01t) - 1$ m.

TABLE I

CLASSIFICATION AND PROPERTIES OF FRICTION MODELS

Friction Model		Duhem type	Rate dependence	Continuity
Dahl	$0 \leq \gamma < 1$	generalized	rate independent	not Lipschitz
	$\gamma = 1$	semilinear	rate independent	Lipschitz
	$\gamma > 1$	generalized	rate independent	Lipschitz
LuGre		generalized	rate dependent	Lipschitz
Maxwell-slip		generalized	rate independent	discontinuous

in Figures 7 and 8 respectively. All three models have similar behavior in the sliding regime, that is, the reversals of the friction force lag velocity sign changes.

VII. CONCLUSION

In this paper we recast the Dahl, LuGre, and Maxwell-slip models as extended, generalized, or semilinear Duhem models. We classified each model accordingly including its rate-independent or rate-dependent behavior. Lipschitz continuity properties of the three friction models were also studied. Table 1 shows the summary of the classification and the properties of the models.

This unified treatment of Duhem-based friction models provides the starting point for further investigations into the relationship between friction modeling and hysteresis. For example, the structure of the Maxwell-slip model as a superposition model suggests that it can be viewed as a variant of the Preisach model [21]–[26]. Allowing the virtual masses in the Maxwell-slip model to possess positive mass should give rise to a rate-dependent presliding-friction model. Finally, by combining these friction models with single- and multi-degree-of-freedom oscillators, we can obtain hysteretic damping models whose frequency-dependent characteristics are more realistic than viscous damping [27].

REFERENCES

[1] B. Armstrong-Hélouvry, *Control of Machines with Friction*. Boston, MA: Kluwer, 1991.

[2] B. Armstrong-Hélouvry, P. Dupont, and C. C. de Wit, "A survey of model, analysis tools and compensation methods for the control of machines with friction," *Automatica*, vol. 30, no. 7, pp. 1083–1138, 1994.

[3] B. Feeny, A. Guran, N. Hinrichs, and K. Popp, "Historical review on dry friction and stick-slip phenomena," *Applied Mechanics Reviews*, vol. 51, no. 5, pp. 321–341, 1998.

[4] P. Dahl, "Solid friction damping of mechanical vibrations," *AIAA J.*, vol. 14, no. 2, pp. 1675–82, 1976.

[5] D. D. Rizos and S. D. Fassois, "Presliding friction identification based upon the Maxwell slip model structure," *Chaos*, vol. 14, no. 2, pp. 431–445, 2004.

[6] V. Lampaert, J. Swevers, and F. Al-Bender, "Modification of the Leuven integrated friction model structure," *IEEE Trans. Autom. Contr.*, vol. 47, no. 4, pp. 683–687, 2002.

[7] C. Canudas de Wit, H. Olsson, K. J. Åstrom, and P. Lischinsky, "A new model for control of systems with friction," *TAC*, vol. 40, no. 3, pp. 419–425, 1995.

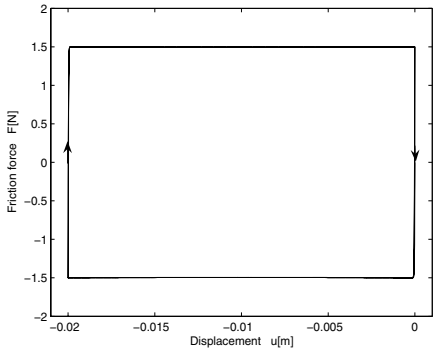

(a)

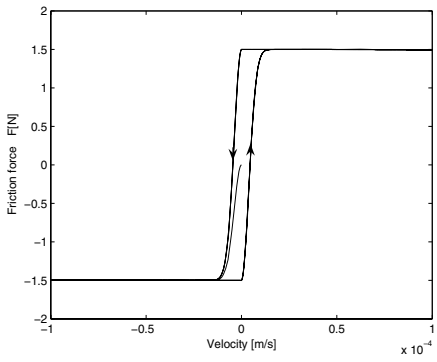

(b)

Fig. 7. (a) Friction force versus displacement and the corresponding (b) friction force versus velocity for the LuGre model (18), (19) with $F_{\rm C} = 1$ N, $F_{\rm S} = 1.5$ N, $v_{\rm S} = 0.001$ m/s, $\sigma_0 = 10^5$ N/m, $\sigma_1 = \sqrt{10^5}$ N-s/m, $\sigma_2 = 0.4$ N-s/m, and $u(t) = 0.01\ (\cos 0.01t) - 1$ m.

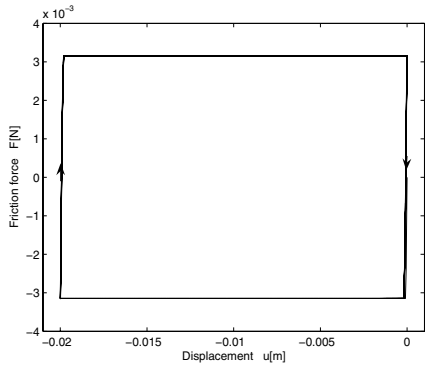

(a)

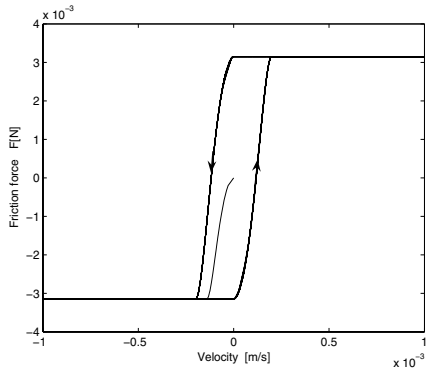

(b)

Fig. 8. (a) Friction force versus displacement and the corresponding (b) friction force versus velocity for the Maxwell-slip model with $N = 10$, $\Delta = [1.5, 2.4, 3.3, 4.2, 5.1, 6, 6.9, 7.8, 8.7, 9.6] \times 10^{-5}$ m, $k = [1, 1.8, 2.6, 3.4, 4.2, 5, 5.8, 6.6, 7.4, 8.2]$ N/m, and $u(t) = 0.01\ (\cos 0.01t) - 1$ m.

[8] J. Swevers, F. Al-Bender, C. G. Ganseman, and T. Prajogo, "An integrated friction model structure with improved presliding behavior for accurate friction compensation," *IEEE Trans. Autom. Contr.*, vol. 45, no. 4, pp. 675–686, 2000.

[9] F. Al-Bender, V. Lampaert, and J. Swevers, "Modeling of dry sliding friction dynamics: From heuristic models to physically motivated models and back," *Chaos*, vol. 14, no. 2, pp. 446–445, 2004.

[10] F. Al-Bender, V. Lampaert, S. D. Fassois, D. D. Rizos, K. Worden, D. Engster, A. Hornstein, and U. Parlitz, "Measurement and identification of pre-sliding friction dynamics," in *Nonlinear Dynamics of Production Systems*. Weinheim: Wiley, 2004, pp. 349–367.

[11] J. Amin, B. Friedland, and A. Harnoy, "Implementation of a friction estimation and compensation technique," *IEEE Contr. Sys. Mag.*, vol. 17, no. 4, pp. 71–76, 1997.

[12] S. C. Southward, C. J. Radcliffe, and C. R. MacCluer, "Robust nonlinear stick-slip friction compensation," *J. Dynamic Systems, Measurement and Control*, vol. 113, no. 4, pp. 639–645, 1991.

[13] S.-W. Lee and J.-H. Kim, "Robust adaptive stick-slip friction compensation," *IEEE Trans. Industrial Electronics*, vol. 42, no. 5, pp. 474–479, 1995.

[14] R.-H. Wu and P.-C. Tung, "Studies of stick-slip friction, presliding displacement, and hunting," *J. Dynamic Systems, Measurement and Control*, vol. 124, no. 1, pp. 111–117, 2002.

[15] M. Marques, *Differential Inclusions in Nonsmooth Mechanical Problems: Shocks and Dry Friction*. Boston, MA: Birkhauser, 1993.

[16] J. Oh and D. S. Bernstein, "Step convergence analysis of nonlinear feedback hysteresis models," in *Proc. Amer. Contr. Conf.*, Portland, OR, 2005, pp. 697–702.

[17] D. Angeli and E. D. Sontag, "Multi-stability in monotone input/output systems," *Sys. Contr. Lett.*, vol. 51, pp. 185–202, 2004.

[18] D. Angeli, J. E. Ferrell, and E. D. Sontag, "Detection of multistability, bifurcations, and hysteresis in a large class of biological positive feedback systems," *Proc. Nat. Academy Sci.*, vol. 101, no. 7, pp. 1822–1827, 2004.

[19] J. Oh and D. S. Bernstein, "Semilinear Duhem model for rate-independent and rate-dependent hysteresis," *IEEE Trans. Autom. Contr.*, vol. 50, no. 5, pp. 631–645, 2005.

[20] P. Dupont, V. Hayward, B. Armstrong, and F. Altpeter, "Single state elasto-plastic friction models," *IEEE Trans. Autom. Contr.*, vol. 47, no. 5, pp. 787–792, 2002.

[21] I. D. Mayergoyz, "Dynamic vector models of hysteresis," *J. Appl. Phys.*, vol. 69, pp. 4829–4834, 1991.

[22] X. Tan and J. S. Baras, "Modeling and control of hysteresis in magnetostrictive actuators," *Automatica*, vol. 40, pp. 1469–1480, 2004.

[23] J. W. Macki, P. Nistri, and P. Zecca, "Mathematical models for hysteresis," *SIAM Review*, vol. 35, no. 1, pp. 94–123, 1993.

[24] I. D. Mayergoyz, *Mathematical Models of Hysteresis*. New York: Springer-Verlag, 1991.

[25] A. Visintin, *Differential Models of Hysteresis*. New York: Springer-Verlag, 1994.

[26] R. B. Gorbet, K. A. Morris, and D. W. L. Wang, "Control of hysteretic systems: A state space approach," in *Learning, Control and Hybrid Systems*. New York: Springer, 1998, pp. 432–451.

[27] A. D. Nashif, D. I. G. Jones, and J. P. Henderson, *Vibration Damping*. New York: Wiley, 1985.